DOI: 10.1002/ejic.200800434

1D, 2D and 3D Coordination Polymers of Aromatic Carboxylate Tb^{III}: Structure, Thermolysis Kinetics and Fluorescence

Ying-Xia Zhou,[a,b] Xiao-Qing Shen,[c] Chen-Xia Du,[a] Ben-Lai Wu,*[a] and Hong-Yun Zhang*[a]

Keywords: Coordination modes / Polymers / Structure elucidation / Kinetics / Fluorescence

Reactions of $TbCl_3 \cdot 6H_2O$ with aromatic acids, namely, pyridine-2,3-dicarboxylic acid (H_2pda), isophthalic acid (H_2ipa) and isonicotinic acid (Hina) gave rise to three new coordination polymers $\{[Tb(pda)(Hpda)] \cdot 3H_2O\}_n$ (**1**), $\{[KTb(ipa)_2(H_2O)_3(\mu\text{-}H_2O)] \cdot 2H_2O\}_n$ (**2**) and $[Tb(ina)_3(H_2O)_2]_n$ (**3**), respectively. Complex **1** constructed by eight-coordinate Tb^{III} nodes connected with completely and half-deprotonated pda and Hpda spacers is a novel 3D metal–organic architecture with nanosized hexagonal 1D channels hosting guest water, whereas complex **2** is a 2D heterometal sheet built by completely deprotonated ipa spacers bridging eight-coordinate K^I and nine-coordinate Tb^{III}. As for **3**, deprotonated monoacid ina anions link eight-coordinate Tb^{III} centres into a 1D double-chain structure. As excited at 320 nm, complexes **1**–**3** all display a serial of emissions centred at about 486, 545, 582 and 620 nm, which is assigned to the characteristic $^5D_4 \rightarrow {}^7F_j$ (j = 6; 5; 4; 3) electronic transitions of Tb^{III}. The overall fluorescence nature of **1**–**3** is extremely alike, but their fluorescence intensity and lifetime are affected by the architectures. Very interestingly, the fluorescence intensity of **2**, especially emitting at 545 nm, is largely enhanced owing to the coordination of alkali metal K^I in the Tb^{III}–carboxylate network. Furthermore, thermal behaviours of **1**–**3** under a nitrogen atmosphere as well as the thermolysis nonisothermal kinetics of **2** are researched.

Introduction

Recently, metal–organic coordination frameworks have received much attention as a new class of materials, because of their intriguing structural features and properties.[1–4] As is well known, aromatic carboxylate ligands with largely rigid frameworks binding elastically coordinating carboxyl groups have been widely selected to assemble with transition metals, and thus a great deal of coordination polymers with novel architectures with potential applications in fields of absorption, separation, sensors and so on have been obtained.[5–10] Comparatively, fewer lanthanide coordination complexes with aromatic carboxylic acid ligands have been investigated, and most of them are discrete molecules.[11–13] Even now lanthanide coordination polymers with aromatic carboxylic acids have stimulated strong interest in light conversion molecular devices.[13–17] Generally, a light conversion process contains the absorption, energy-transfer, emission sequence involving distinct absorbing (the ligand) and emitting (the lanthanide ion) components. However, the absorption ability of lanthanides for ultraviolet light is very weak,[17] and therefore, the luminescent intensities of lanthanide complexes are intensely dependent on the organic ligands used.[18–22] Commonly, due to possessing large conjugated π-electron systems and strong carboxyl absorption groups, aromatic carboxylic acids are good activators for the luminescence of lanthanide ions.[23–29] For example, when coordinated with dipicolinic acid, terbium(III) and europium(III) complexes have good luminescent properties because of highly efficient light conversion, which enhances the luminescence intensities up to 10^4-fold.[27] Another interesting case firstly reported by Peng Cheng et al. is the pyridine-2,6-dicarboxylate-bridged luminescent 3D nanoporous polymers with d–f mixed metals. Those coordination polymers have 1D channels and their luminescence displays high-performance selectivity for Zn^{II}.[30] In this paper, we selected pyridine-2,3-dicarboxylic acid (H_2pda), isophthalic acid (H_2ipa) and isonicotinic acid (Hina) as linkers to assemble with lanthanide Tb^{III}, and we expected that not only the structural diversity but also the luminescence properties of the resultant complexes could be tuned by changing the nature of the carboxyl groups on the aromatic ring (Scheme 1). As a result, three new coordination polymers of Tb^{III}, namely, $\{[Tb(pda)(Hpda)] \cdot 3H_2O\}_n$ (**1**), $\{[KTb(ipa)_2(H_2O)_3(\mu\text{-}H_2O)] \cdot 2H_2O\}_n$ (**2**) and $[Tb(ina)_3(H_2O)_2]_n$ (**3**), were obtained. Structural analyses show that complex **1** is a

[a] Department of Chemistry, Zhengzhou University, Zhengzhou 450052, P. R. China
E-mail: wzhy917@zzu.edu.cn
wbl@zzu.edu.cn
[b] College of Science, Henan Agricultural University, Zhengzhou 450052, P. R. China
[c] College of Material Engineering, Zhengzhou University, Zhengzhou 450052, P. R. China

Supporting information for this article is available on the WWW under http://www.eurjic.org or from the author.

novel 3D metal–organic architecture with 1D channels, whereas complex **2** is a 2D heterometal sheet and complex **3** is a 1D double-chain structure. The overall nature of fluorescence of **1**–**3** is extremely alike, but their fluorescence intensity and lifetime are affected by the architectures of the ligands. Very interestingly, the fluorescence intensity of **2**, emitting at 545 nm, is largely enhanced owing to the coordination of alkali metal K^I in the Tb^{III}–carboxylate network. Moreover, we also wish to report their thermal stability measurements and thermolysis kinetics analyses. On the basis of the results of thermal analyses, the kinetic parameters of thermal decomposition were fitted by the Ozawa–Flynn–Wall equation.

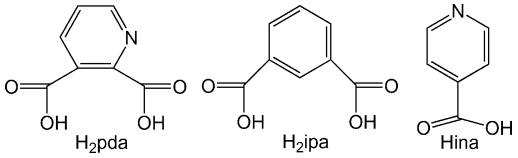

Scheme 1. Schematic representation of the selected ligands: pyridine-2,3-dicarboxylic acid (H_2pda), isophthalic acid (H_2ipa) and isonicotinic acid (Hina).

Results and Discussion

Description of the Crystal Structures

{[Tb(pda)(Hpda)]·3H$_2$O}$_n$ (1)

As shown in Figure 1, each Tb^{III} centre in **1** is in an eight-coordinate environment of N_2O_6 ligated by two completely deprotonated pda spacers and two-half deprotonated Hpda spacers, but it is structurally uncertain as to which ligand bears the protonated carboxyl group. The Tb1–O1 and Tb1–O4 bond lengths are 2.333(5) and 2.311(5) Å, respectively, and they are slightly shorter than the Tb1–O3B and Tb1–O3C bonds [2.487(4) Å], but slightly longer than the Tb1–O6A and Tb1–O6B bonds [2.302(4) Å]. All the Tb–O bond lengths are consistent with literature values.[12b,23] The Tb1–N1 and Tb1–N2 bond lengths are 2.564(7) and 2.577(6) Å, respectively, which are notably longer than those of Tb–O. In the crystal structure, the pyridine-2,3-dicarboxylate ligands have two coordinated modes: one half ligands act as T-shaped three-connectors by using the nitrogen atom and one oxygen atom of the 2-carboxyl group to chelate one Tb^{III} and two oxygen atoms of the 3-carboxyl group to bridge the other two Tb^{III}, and in this manner, ladder-like 1D chain subunits shown in Figure 2 are formed. The other half ligands act as linear brid-

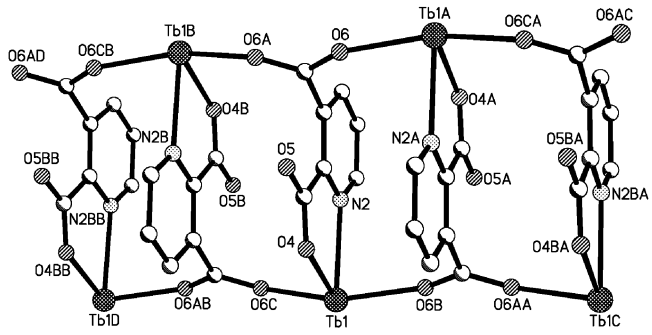

Figure 2. View of the ladder-like 1D chain along the *b* axis for **1**.

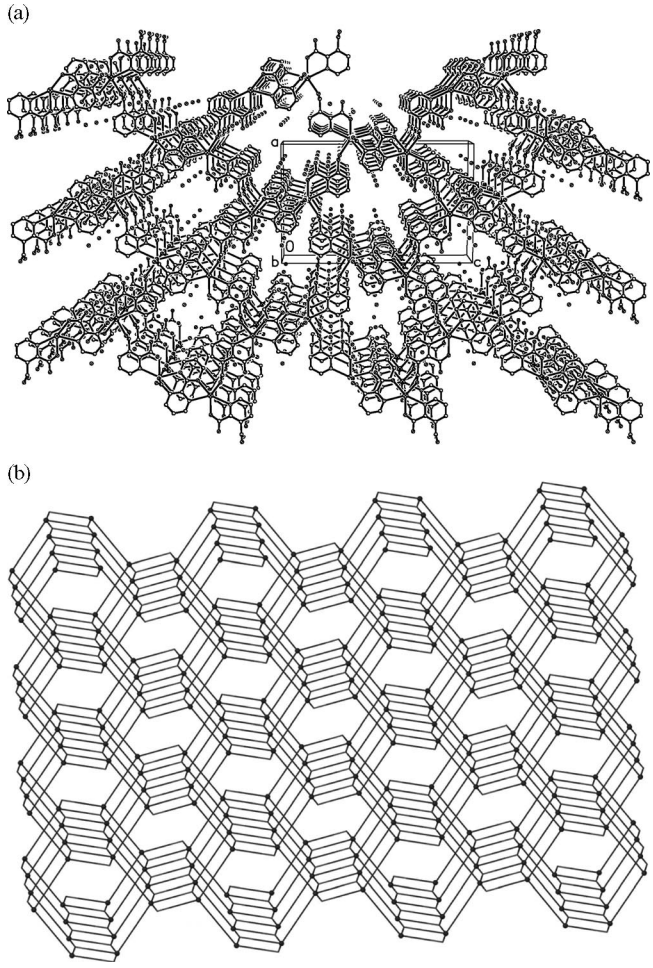

Figure 3. (a) View of the 3D network showing water molecules occupying the 1D channel of **1** and (b) a simplified scheme indicating the construction of **1**.

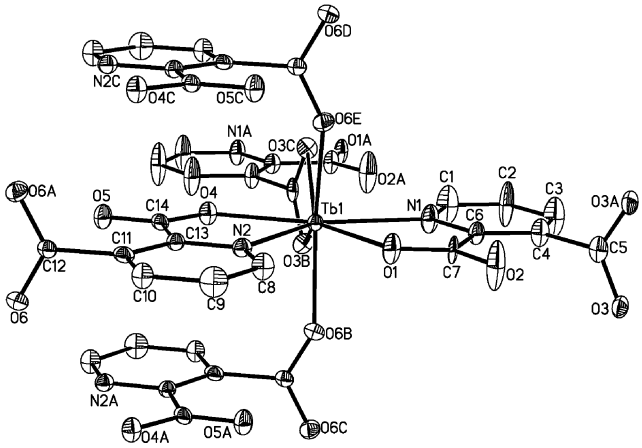

Figure 1. ORTEP drawing of the coordination geometry around Tb^{III} in **1**; H atoms are omitted for clarity.

ges with the nitrogen atom and one oxygen atom of the 2-carboxyl group chelating one Tb^{III} in one subunit chain and the 3-carboxyl groups chelating the other Tb^{III} in other subunit chains, and finally, those 1D chain subunits are linked into a 3D porous framework. As clearly shown in Figure 3a, the porous framework has nanosized puckered hexagonal channels occupied by free water molecules along the *b* axis, and the total potential solvent area volume calculated by Platon is about 41.7%. The interesting construction of the 3D network in **1** is further simplified in Figure 3b. T-shaped spacers threefold connect Tb^{III} ions into 1D ladder-like chains, where the metal separations are 7.377 and 6.322 Å, whereas linear spacers couple those ladder-like chains into the porous network with a metal separation of 8.708 Å, indicating the key role of the pyridine-2,3-dicarboxylate coordination models upon the resulting architecture.

{[KTb(ipa)$_2$(H$_2$O)$_3$(μ-H$_2$O)]·2H$_2$O}$_n$ (2)

Compound **2** is a heteronuclear complex of isophthalate and Tb^{III} and K^{I}. The coordination environments of Tb^{III} and K^{I} are shown in Figure 4. The asymmetric unit of **2** consists of one Tb^{III}, one K^{I}, two ipa ligands, four coordination water molecules and two lattice water molecules. The coordination geometry around every Tb^{III} centre is formed by Tb^{III} connecting with four oxygen atoms of two chelate carboxyl groups from two ipa ligands, two oxygen atoms from another two ipa ligands and three oxygen atoms from one monodentate and two bridging water molecules, whereas the coordinated sphere around each K^{I} is constructed through K^{I} coordinating with five oxygen atoms from five ipa ligands and three oxygen atoms from two bridging and one monodentate water molecule. The Tb–O bond lengths formed with monodentate or bridging carboxyl groups are in the range from 2.334 to 2.379 Å, which is in agreement with literature values,[23] whereas the Tb–O bond lengths formed with chelate carboxyl groups are in the range 2.420–2.710 Å, which are longer than those reported in the literature.[23] The Tb–O_w distances are in the range 2.334–2.553 Å, which are also larger than those of literature values.[23] The K–O distances are in the range 2.765–3.009 Å, which are consistent with literature values.[31] Due to both Tb^{III} and K^{I} adopting a high coordination number and being surrounded by several ipa ligands, the coordination environments largely deviate from either tricapped trigonal prismatic or monocapped square antiprismatic geometries often met in the same spheres of the coordination number.[23] In **2**, isophthalates have two coordination modes: one as a four connector uses one carboxyl group to chelate one Tb^{III} and bridge two K^{I} ions, and the other carboxyl group to coordinate a K^{I} in a monodentate fashion; the other as a six connector utilizes one carboxyl group to chelate one Tb^{III} and bridge two K^{I} ions in the above-mentioned coordination mode and the other carboxyl group to bridge two Tb^{III} and one K^{I}. Consequently, a 2D heteronuclear comb-like network of isophthalate is created (shown in Figure 5). Very interestingly, guest water molecules between adjacent sheets are connected with coordinated and uncoordinated water molecules and chelated or bridged coordinated oxygen atoms of the isophthalate to form a complicated hydrogen-bonding network (seen in Scheme 2 and Table 1). As a result, the 2D sheets extend into a 3D supramolecular framework (shown in Figure 6).

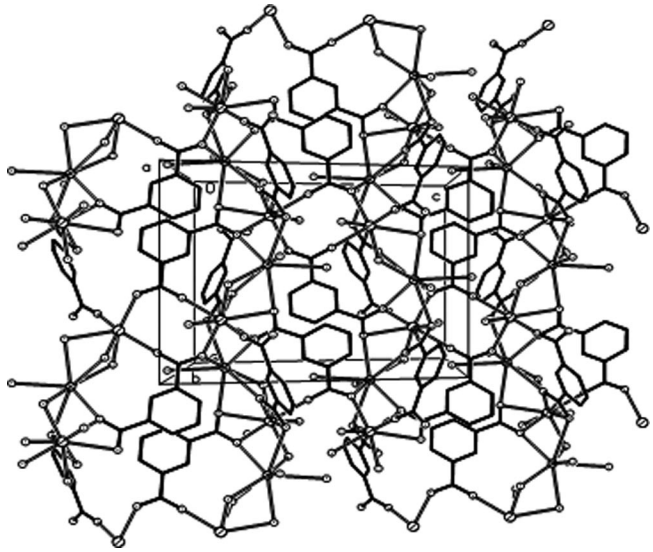

Figure 5. Drawing of the 2D framework of **2**.

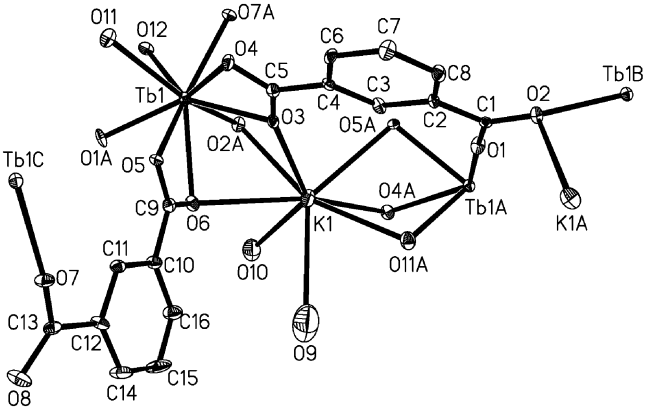

Figure 4. ORTEP drawing of the coordination geometries of Tb^{III} and K^{I} in **2**; H atoms are omitted for clarity.

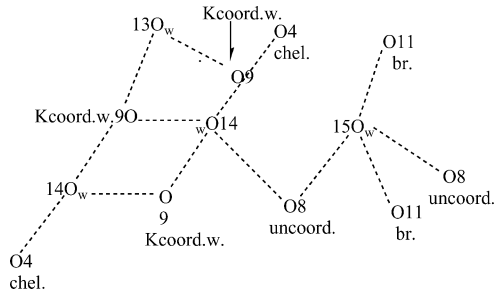

Scheme 2. Schematic presentation of hydrogen-bonding network in **2** ($O_w14\cdots O_w9$ 2.812 Å, $O_w14\cdots O8_{uncoord.}$ 2.813 Å, $O_w14\cdots O4_{chel.}$ 2.788 Å, $O_w15\cdots O8_{uncoord.}$ 2.802 Å, $O_w15\cdots O11_{br.}$ 2.831 Å, $O_w13\cdots O_w9$ 2.721 Å).

Table 1. Hydrogen bond lengths [Å] for complexes **2** and **3**.

Complex **2**		Complex **3**	
O_w14–H···O_w9	2.812	O1–H···O2	3.018
O_w14–H···O8	2.813	O1–H···N1	2.934
O_w14–H···O4	2.788	O1–H···N2	2.811
O_w15–H···O8	2.802		
O_w15–H···O11	2.831		
O_w13–H···O_w9	2.721		

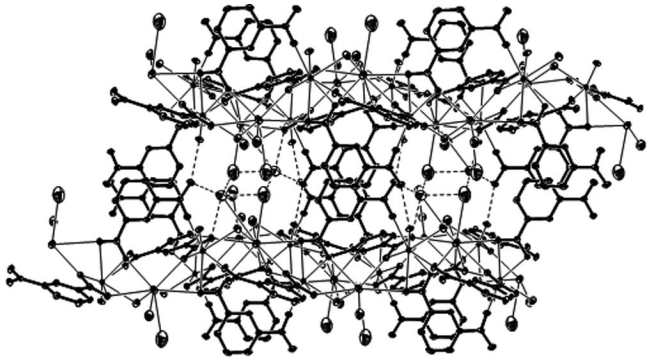

Figure 6. Drawing of the hydrogen-bonding 3D supramolecular framework in **2**.

[Tb(ina)$_3$(H$_2$O)$_2$]$_n$ (3)

Complex **3** crystallizes in a monoclinic space group *C*2/*c* and the coordination environment centre nodes Tb^{III} is shown in Figure 7. The asymmetric unit of **3** consists of one Tb^{III}, three isonicotinate and two coordination water molecules. The eightfold coordinated sphere around every Tb^{III} is a distorted square antiprismatic geometry constructed by four oxygen atoms from four bridging isonicotinates, two oxygen atoms from one chelate isonicotinate and two oxygen atoms from water coordinating with Tb^{III}. The Tb–$O_{carboxyl}$ distances are in the range 2.293–2.460 Å, which are consistent with literature values,[12b] and the average Tb–O_w distance is 2.416 Å, which is longer than the literature value.[12b] In **3**, isonicotinates display two coordinating modes, namely, chelating and bridging coordination models of carboxyl groups without the nitrogen atoms of the pyridyl groups taking part in the coordination. The overall structural feature of **3** is a 1D two-stranded chain (seen in Figure 8) constructed from two isonicotinates simultaneously bridging adjacent two Tb^{III} side by side and two isonicotinates chelating them up and down with a metal separation of 4.951 Å. In the crystal structure there are two hydrogen bonds (seen in Table 1). The coordination water with the neighbouring oxygen atom of the chelating carboxyl form weakly intramolecular hydrogen bonds with O1···O2 of 3.018 Å, and coordination water with the $N_{pyridyl}$ of the neighbouring chain form intermolecular hydrogen bonds with O1···N1 of 2.934 Å and O1···N2 of 2.811 Å. Thus, those two-stranded chains are connected with neighbouring chains by intermolecular hydrogen bonds to form a 3D supramolecular framework in **3** (Figure 9).

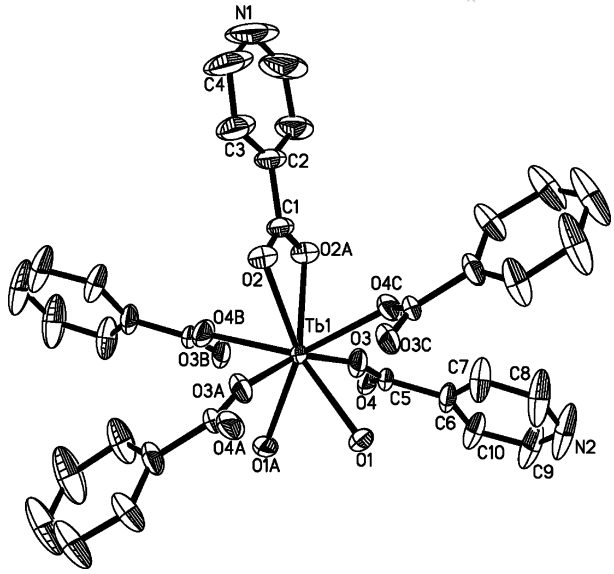

Figure 7. ORTEP drawing of the structural unit of **3**.

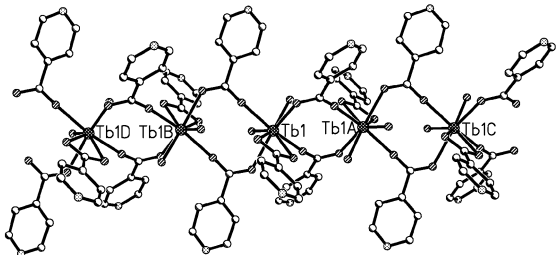

Figure 8. Drawing of the 1D double chain in **3**.

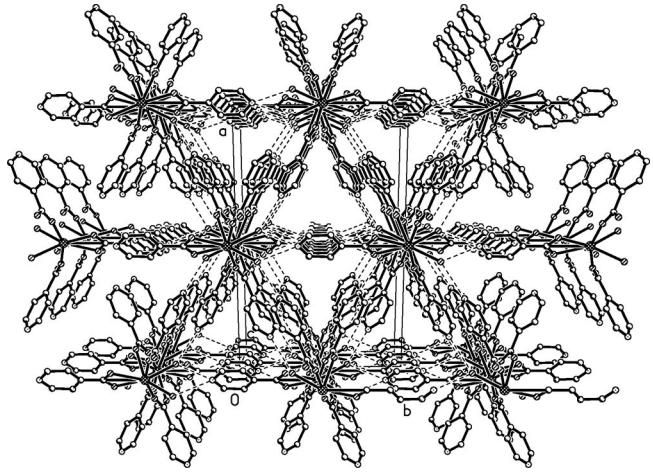

Figure 9. Drawing of the 1D chain hydrogen bonding into a 3D framework in **3**.

From comparison of complexes **1**, **2** and **3**, it is seen that their structures have very large difference. Complex **1** possesses a 3D framework with many water molecules acting as guests in the hosting cavities, **2** is a 2D framework with some water molecules as guests residing between sheets and **3** has a 1D double-stranded chain structure without lattice water molecules. Certainly, the structure diversities mainly

result from the features of the ligands, although there are only slight differences among the pda, ipa and ina ligands. Other important factors can be attributed to the coordination lability of the carboxylic groups and further hydrogen-bonding assemblies.[32]

Thermal Decomposition of Complexes 1, 2 and 3 and Nonisothermal Kinetics of the Thermal Decomposition of 2

The typical TG and DTG curves of complex **2** are shown in Figure 10. It can be seen that there are three transitions that appear in the decomposition process. The first transition, which starts at 28 °C and ends at 85 °C, is due to the loss of lattice water molecules. The second transition ranging from 215 to 295 °C is a main process containing an exothermic peak at 275 °C. This thermal event has a mass loss of 24.9% and results from decomposition of **2**. The third transition occurred from 445 to 620 °C with a DTG peak at 575 °C and is related to the gradual elimination of carbon deposition resulting from the complex decomposition under a N_2 atmosphere.[33] The total mass loss up to 700 °C is 65.9%, which almost agrees with the theoretical value (68.3%) calculated by taking Tb and K as the final products.

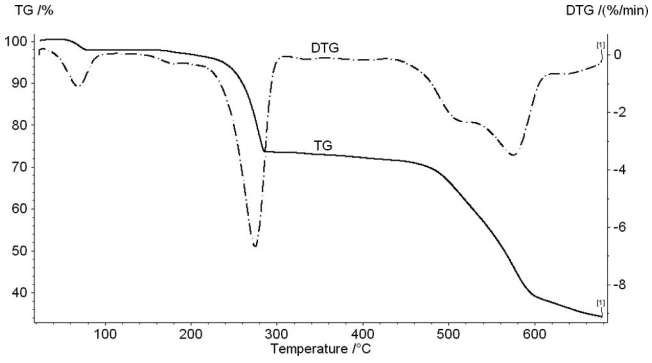

Figure 10. TG–DTG curves of **2**.

The TG and DTG curves of complexes **1** and **3** are similar to that of complex **2**. However, there are three transitions appearing in the decomposition process of **1** and two transitions appearing in the decomposition process of **3**. The last transitions of **1** and **3** are also all the gradual elimination of carbon deposition. Complex **1** loses three lattice H_2O molecules between 30 and 195 °C, and its decomposition occurs between 225 and 316 °C. The total weight loss is about 65.3% (calculated by taking Tb as the final products, 70.7%). Complex **3** decomposes at 200–270 °C and the total mass loss up to 700 °C is 68.3% (calculated by taking Tb as the final products, 72.5%).

Nonisothermal kinetics of complex 2

The TG curves for the decomposition of complex **2** from 25 to 350 °C with a heating rate of 10, 15, 20 and 30 °C min^{-1} were recorded, and a series of dynamic scans with different heating rates results in a set of data that exhibits the same degree of conversion (α) at different temperatures. The basic data (β, α, T) taken from the TG curves are used in the equations bellow:

Ozawa–Flynn–Wall (OFW) equation[34]

where β is the heating rate, α is the degree of conversion, $g(\alpha)$ is a mechanism function, E is the activation energy, A is a preexponential factor and R is the gas constant.

From Equation (1) it can be seen that the $\ln\beta$ vs. $1/T$ plots show straight lines with slopes $m = -1.052E/R$. The slopes of these straight lines are directly proportional to the reaction activation energy (E). Figure 11 shows these lines at different α. The calculated results of the first and the second transition by using Equation (1) are listed in Table 2.

$$\ln\beta = \ln\left(\frac{AE}{R}\right) - \ln g(\alpha) - 5.3305 - 1.052\left(\frac{E}{RT}\right) \quad (1)$$

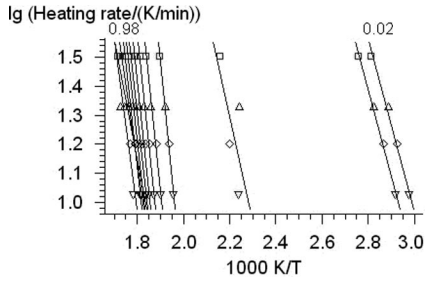

Figure 11. OFW analysis of **2**.

Table 2. Kinetic parameters for the thermal decomposition of **2**.

Partial Mass Loss	E [kJ mol^{-1}]	log (A [s^{-1}])
0.02	58.36 ± 4.88	5.89
0.05	51.45 ± 3.05	4.80
0.10	122.86 ± 7.36	10.66
0.20	132.83 ± 21.16	10.55
0.30	136.37 ± 21.95	10.94
0.40	134.00 ± 21.60	10.75
0.50	129.23 ± 23.47	10.36
0.60	126.74 ± 23.37	10.20
0.70	122.73 ± 23.97	9.91
0.80	110.55 ± 27.73	8.89
0.90	87.50 ± 31.30	6.89
0.98	145.04 ± 80.62	11.87

The dependence of the activation energy on the degree of conversion (E_α-dependence) given in Table 2 shows that the activation energy is not a constant. According to the OFW method, the activation energies and pre-exponential factors of thermal decomposition for the first and second transition are: $E_1 = 136.37 \pm 21.95$ kJ mol^{-1}, $\log(A_1/s^{-1}) = 10.94$, $E_2 = 112.06 \pm 24.21$ kJ mol^{-1}, $\log(A_2/s^{-1}) = 8.88$.

UV/Vis Spectra

The UV/Vis spectra of complex **1** in DMF and complexes **2** and **3** in methanol and their free ligands in DMF or methanol were determined (Figure 12). All complexes

exhibit domain absorption peaks in the narrow ultraviolet region from 200 to 300 nm, which is attributed to the characteristic absorption of the π–π * transition of the aromatic ring and are similar to the absorption bands of the free ligand, except for complex **1**. This indicates that the aromatic rings in the ipa and ina ligands do not coordinate to the Tb^{III} ions in complex **2** and **3**,[12b] but in complex **1**, two absorption bands are blueshifted relative to the free pda ligand probably due to the nitrogen atom of the pyridine ring in the pda ligand coordinated to the Tb^{III} ions, which results in an electron cloud excursion from the phenyl ring to the Tb^{III} ion and extension of the conjugation system.[12b] The UV/Vis results show that ligands in complexes **1**, **2** and **3** are the energy donors and luminescence sensitizer of the Tb^{III} ions.

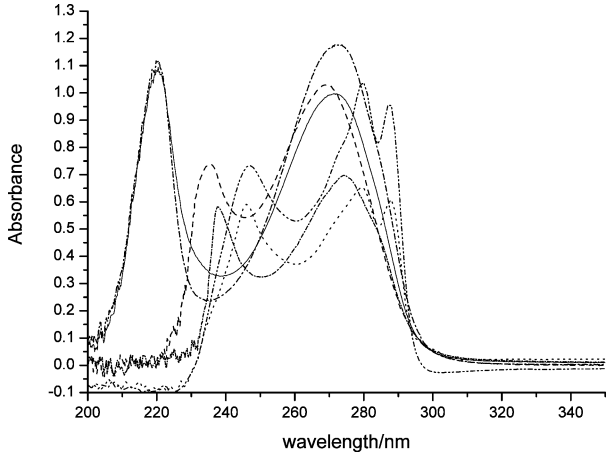

Figure 12. UV absorption spectra of H_2pda, H_2ipa and Hina and complexes **1**, **2** and **3** (short dash dot, H_2pda; dash, complex **1**; dash dot dot, H_2ipa; dot, complex **2**; solid Hina; dash dot, complex **3**).

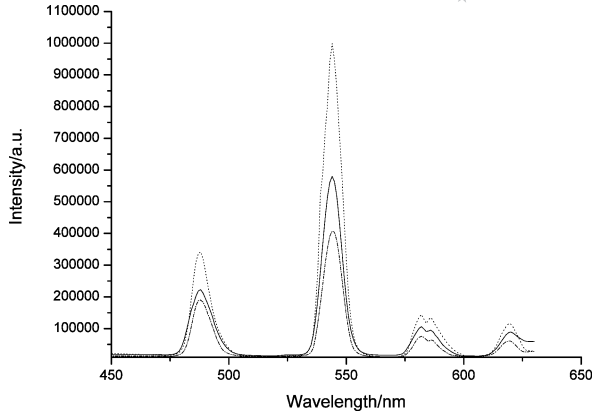

Figure 13. Fluorescence emission spectra of complexes **1**, **2** and **3** (solid, complex **1**; dot, complex **2**; dash dot, complex **3**).

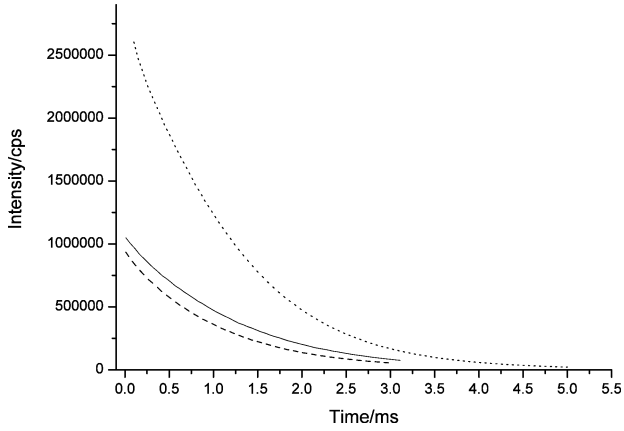

Figure 14. Phosphorescence lifetime curves of complexes **1**, **2** and **3** (dash, complex **1**; solid, complex **2**; dot, complex **3**).

Photoluminescence

Under the excitation of 320 nm UV light, complexes **1**, **2** and **3** all exhibit an intense green luminescence. Their solid-state fluorescence spectra are shown in Figure 13 and the phosphorescence lifetime (Figure 14) were also determined.

For complexes **1**, **2** and **3**, the positions of their emission bands at about 486, 545, 582 and 620 nm (see Figure 13) all are similar, which are assigned to the $^5D_4 \rightarrow {}^7F_6$, $^5D_4 \rightarrow {}^7F_5$, $^5D_4 \rightarrow {}^7F_4$ and $^5D_4 \rightarrow {}^7F_3$ electronic transitions of the Tb^{III} ion, respectively. The band at about 545 nm is more intense than the others, which is consistent with the observation that the $^5D_4 \rightarrow {}^7F_5$ transition is the preferred transition of terbium-containing materials.[35] The splitting of the weak peak at 582 nm is due to crystal-field splitting.[36]

As showed in Figure 13, the relative luminescence intensity of complex **2** is much stronger than that of complexes **1** and **3**, and complex **2** also displays a longer phosphorescence lifetime (2.76 ms) than **1** (2.52 ms) or **3** (2.37 ms). That is, the luminescence performance of **2** is the best among the three complexes. This phenomenon may be attributed to the K^I ion existing in the crystal structure of **2**. It is well known that the luminescent intensity of Ln^{III} relies on the efficiency of the energy transfer from the ligand to the Ln^{III} centre.[37] According to this, the enhancement in the luminescent intensity and phosphorescence lifetime of **2** may result from a more effective intramolecular energy transfer from the ipa ligand to the Tb^{III} ion when K^I exists in the structure.[30] That is, for the structure of **2** the lowest triplet state energy level of the ligand and the lowest exited state energy level of the Tb^{III} ions are better matched than they are in the structures of **1** and **3**.

As for complexes **1** and **3**, the luminescence performance (fluorescence intensity and phosphorescence lifetime) of **1** is better than that of **3**. This phenomenon can be attributed to two aspects. First, around the Tb^{III} centre, **1** has no coordination water molecule, but **3** has two coordinated water molecules. As is known,[38] the coordination of water molecule would decrease the fluorescence intensity of a rare-earth metal complex because the thermal vibration of water molecules would consume part of the energy absorbed by the ligand. Moreover, the coordination model between the ligands and the Tb^{III} ions may be an important factor that

influences the luminescence properties of the complex, because it can influence the matching of the lowest triplet state energy level of the ligand to the lowest excited state energy level of the Tb^{III} ion.[39] The lowest triplet state energy level of the ligand and the lowest excited state energy level of the Tb^{III} ion may be better matched, because each Tb^{III} ion may be chelated by more ligands in the structure of the complex.[39] As discussed above, the number of ligands that are coordinated to Tb^{III} through bidentate chelate rings is larger in **1** (3) than that in **3** (1). So, the energy matching leads to a better luminescence performance of **1** than **3**.

B. Zhao et al.[30] found that the fluorescence intensity of the coordination polymer $\{[Tb(PDA)_3Mn_{1.5}(H_2O)_3]\cdot 3\cdot 25H_2O\}_\infty$ with a 1D channel (PDA = pyridine-2,6-dicarboxylic acid) increased significantly upon the addition of Zn^{II} in DMF solvent, whereas the introduction of other metal ions caused the intensity to be either unchanged or weakened. The case reveals that this polymer could monitor or recognize Zn^{II} to some extent and be considered as a luminescent probe. As shown in Figure 13, the highest fluorescence peak at 545 nm of complex **2** is almost twice as intense as the corresponding band of **1** and three times that of **3**. The result shows that K^I in the structure of complex **2** improves the luminescent performance of **2**, which may provide an opening into a promising new field in luminescent materials. Therefore, it is worthwhile to study further the luminescent properties of more heterometallic lanthanide complexes in our future research.

Conclusions

Complexes **1**, **2** and **3** possess different structures due to the diversity of their ligands, although there are only slight differences among the pda, ipa and ina ligands. Complex **1** possesses a 3D framework with a ladder-like shape along the *b* axis, **2** is a 2D sandwich and **3** has a 1D double-stranded chain structure. There are many lattice water molecules in complexes **1** and **2**, but none in **3**.

Complex **1** is the most stable among the three complexes, whereas complex **3** is the least stable, which is perhaps because complexes **1**, **2** and **3** possess 3D, 2D and 1D frameworks, respectively. Kinetic analysis shows the decomposition mechanism of complex **2** is a two-step reaction with E_1 = 112.06 kJ mol^{-1}, E_2 = 109.60 kJ mol^{-1}, $\log(A_1/s^{-1})$ = 16.80, $\log(A_2/s^{-1})$ = 8.83. These values would offer initial values for getting reaction model and for the further research work of complex **2**.

The relative fluorescence intensity of complex **2** is much stronger than that of complexes **1** and **3**, because K^I exists in the crystal structure of **2**, which can be attributed to more effective intramolecular energy transfer from the ipa ligand to the Tb^{III} centre. This result is important for the application of this material as a fluorescent probe.

Experimental Section

Materials and Physical Measurements: Pyridine-2,3-dicarboxylic acid was purchased in analytical pure grade from Alfa Aesar, and

Table 3. Crystal data and structure refinement for complexes **1**, **2** and **3**.

Complex name	Complex **1**	Complex **2**	Complex **3**
Empirical formula	$C_{14}H_{12}N_2O_{11}Tb$	$C_{16}H_8K\ O_{14}\ Tb$	$C_{18}H_{12}\ N_3\ O_8\ Tb$
Formula weight	543.18	622.24	557.23
Temperature [K]	293(2)	291(2)	291(2)
Wavelength [Å]	0.71073	0.71073	0.71073
Crystal system	Orthorhombic	Monoclinic	Monoclinic
Space group	*Pnma*	*C*2/*c*	*C*2/*c*
a [Å]	14.239(3)	22.262(5)	20.311(4)
b [Å]	6.7220(13)	12.667(3)	11.639(2)
c [Å]	22.880(5)	16.121(3)	9.885(2)
α [°]	90	90	90
β [°]	90	112.21(3)	115.65(3)
γ [°]	90	90	90
V [Å^3]	2190.0(7)	4209.0(15)	2106.7(7)
Z	4	8	4
$D_{calcd.}$ [Mg m^{-3}]	1.647	1.964	1.757
μ [mm^{-1}]	3.281	3.629	3.405
F(000)	1052	2400	1080
Crystal size [mm]	0.20 × 0.20 × 0.10	0.20 × 0.15 × 0.10	0.30 × 0.20 × 0.20
θ [°]	3.00 to 25.00	1.89 to 26.50	2.07 to 27.52
Limiting indices	$-16 \le h \le 0$	$-27 \le h \le 13$	$-26 \le h \le 11$
	$-7 \le k \le 0$	$-15 \le k \le 13$	$-15 \le k \le 13$
	$-27 \le l \le 27$	$-18 \le l \le 20$	$-11 \le l \le 12$
Reflections collected/ unique	3550/1918 [*R*(int) = 0.0596]	7045/4083 [*R*(int) = 0.0524]	4003/2298 [*R*(int) = 0.0384]
Data/restraints/param.	1918/0 /163	4083/0/291	2298/0/139
Goodness-of-fit on F^2	1.053	1.041	1.080
*R*1	0.0471	0.0403	0.0381
*wR*2	0.0930	0.0878	0.0863
$\Delta\rho$(min, max) [e Å^{-3}]	1.166, –1.345	1.230, –1.007	0.804, –0.691

$TbCl_3·6H_2O$ was prepared by treating the terbium oxide (Tb_4O_7) with concentrated hydrochloric acid according to a conventional method.[40] Other reagents and solvents were reagent grade, which were purchased from Zhengzhou Zhongliang Chemical Reagent Company, and used without purification. Single crystal structures were measured with a Rigaku-Raxis-IV X-ray diffractometer. IR spectra were recorded with a FTS-40 infrared spectrophometer as KBr pellets in the 4000–400 cm^{-1} region. Thermal decomposition experiments were carried out by using a NETZSCH TG 209 instrument under a nitrogen atmosphere from room temperature to 700 °C with a flow rate of 20 mL min^{-1}. The heating rate for thermal decomposition was 10 °C min^{-1}, and the rates for thermal decomposition kinetic analysis were 10, 15, 20 and 30 °C min^{-1}, respectively. Ultraviolet absorption spectra were measured using an Agilent 8453 spectrophotometer. The luminescence (excitation and emission) spectra for the powdered complexes samples were determined with a Fluoro Max-p spectrophotometer at room temperature: excitation wavelength = 320 nm, delay time = 0.01 ms, scan speed = 1000 nm/s, excitation and emission slit width = 0.5 nm, and the phosphorescence lifetimes were measured with an excitation wavelength of 545 nm.

$\{[Tb(pda)(Hpda)]·3H_2O\}_n$ (1): A solution of $TbCl_3·6H_2O$ (0.8959 g, 2.4 mmol) in water (10 mL) was added dropwise to a solution of pda (1.2358 g, 7.4 mmol) dissolved in 10% ammonia liquor (20 mL) with stirring, and the solution was continuously stirred for 20 min. A white precipitate was formed in the reaction mixture, which was filtered. The filtrate was left undisturbed and allowed to evaporate at ambient temperature over a period of 4 weeks, which afforded colourless block crystals suitable for X-ray single-crystal diffraction analysis after filtering and washing with ethanol. Yield: 0.326 g (25%). IR (KBr): $\tilde{\nu}$ = 3335 (m), 3151 (m), 1730 (m), 1610 (s), 1578 (s), 1473 (m), 1453 (s), 1397 (s), 448 (w) cm^{-1}.

$\{[KTb(ipa)_2(H_2O)_3(\mu\text{-}H_2O)]·2H_2O\}_n$ (2): A solution of $TbCl_3·6H_2O$ (0.746 g, 2 mmol) in water (10 mL) was added dropwise to a solution of potassium isophthalate (1.218 g, 6 mmol) dissolved in water (5 mL) and acetonitrile (15 mL) with stirring. The reaction mixture was heated at 60 °C and stirred for 30 min with a magnetic stirrer. A white precipitate appeared, which was left overnight and then filtered. The filtrate was left undisturbed and allowed to evaporate at ambient temperature over a period of 2 months, which afforded colourless stick crystals suitable for X-ray single crystal diffraction

Table 4. Selected bond lengths [Å] for complexes **1**, **2** and **3**.

Complex **1**		Complex **2**		Complex **3**	
Tb1–O6A	2.305(3)	Tb1–O7A	2.334(3)	Tb1–O3A	2.293(4)
Tb1–O6B	2.305(3)	Tb1–O2B	2.365(3)	Tb1–O3	2.293(4)
Tb1–O4	2.319(5)	Tb1–O1C	2.379(3)	Tb1–O4B	2.385(2)
Tb1–O1	2.342(4)	Tb1–O3	2.420(3)	Tb1–O4C	2.385(2)
Tb1–O3C	2.489(3)	Tb1–O5	2.463(3)	Tb1–O1A	2.416(3)
Tb1–O3D	2.489(3)	Tb1–O11	2.523(3)	Tb1–O1	2.416(3)
Tb1–N1	2.563(6)	Tb1–O12	2.553(3)	Tb1–O2	2.460(2)
Tb1–N2	2.585(5)	Tb1–O6	2.563(3)	Tb1–O2A	2.460(2)
		Tb1–O4	2.710(3)		
		K1–O3	2.765(3)		
		K1–O2B	2.772(3)		
		K1–O4A	2.844(3)		
		K1–O5A	2.866(3)		
		K1–O11A	2.913(3)		
		K1–O10	2.975(4)		
		K1–O6	3.009(3)		
		K1–O9	3.143(6)		

Table 5. Selected bond angles [°] for complexes **1**, **2** and **3**.

Complex **1**[a]			
O6A–Tb1–O6B	156.3(2)	O3C–Tb1–O3D	52.49(18)
O6A–Tb1–O4	93.59(10)	O6A–Tb1–N1	91.53(10)
O6B–Tb1–O4	93.59(10)	O6B–Tb1–N1	91.53(10)
O6A–Tb1–O1	80.02(10)	O4–Tb1–N1	154.8(2)
O6B–Tb1–O1	80.02(10)	O1–Tb1–N1	65.04(19)
O4–Tb1–O1	140.16(18)	O3C–Tb1–N1	80.92(16)
O6A–Tb1–O3C	128.07(14)	O3D–Tb1–N1	80.92(16)
O6B–Tb1–O3C	75.59(14)	O6A–Tb1–N2	81.32(9)
O4–Tb1–O3C	76.52(15)	O6B–Tb1–N2	81.32(9)
O1–Tb1–O3C	137.21(13)	O4–Tb1–N2	65.06(19)
O6A–Tb1–O3D	75.59(14)	O1–Tb1–N2	75.10(19)
O6B–Tb1–O3D	128.07(14)	O3C–Tb1–N2	133.40(15)
O4–Tb1–O3D	76.52(15)	O3D–Tb1–N2	133.40(15)
O1–Tb1–O3D	137.21(13)	N1–Tb1–N2	140.1(2)
Complex **2**[b]			
O7A–Tb1–K1	100.05(8)	O2B–Tb1–K1	42.62(7)
O7A–Tb1–O2B	84.46(10)	O1C–Tb1–K1	111.71(7)
O7A–Tb1–O1C	137.94(11)	O3–Tb1–K1	42.72(7)
O2B–Tb1–O1C	100.41(10)	O5–Tb1–K1	88.14(7)
O7A–Tb1–O3	80.14(10)	O11–Tb1–K1	165.43(7)
O2B–Tb1–O3	77.08(10)	O12–Tb1–K1	119.06(7)
O1C–Tb1–O3	141.84(10)	O6–Tb1–K1	48.73(7)
O7A–Tb1–O5	134.96(10)	O4–Tb1–K1	92.77(7)
O2B–Tb1–O5	125.88(9)	O3–K1–O2B	65.17(8)
O1C–Tb1–O5	74.66(10)	O3–K1–O4A	139.30(9)
O3–Tb1–O5	76.54(10)	O2B–K1–O4A	109.72(9)
O7A–Tb1–O11	82.83(10)	O3–K1–O5A	79.75(9)
O2B–Tb1–O11	151.66(10)	O2B–K1–O5A	91.35(9)
O1C–Tb1–O11	73.36(10)	O4A–K1–O5A	59.68(8)
O3–Tb1–O11	125.07(10)	O3–K1–O11A	101.82(9)
O5–Tb1–O11	79.97(10)	O2B–K1–O11A	157.33(9)
O7A–Tb1–O12	70.80(10)	O4A–K1–O11A	67.11(9)
O2B–Tb1–O12	76.50(10)	O5A–K1–O11A	67.35(8)
O1C–Tb1–O12	69.92(10)	O3–K1–O10	130.94(10)
O3–Tb1–O12	142.17(10)	O2B–K1–O10	74.98(10)
O5–Tb1–O12	141.28(9)	O4A–K1–O10	79.85(10)
O11–Tb1–O12	75.43(10)	O5A–K1–O10	130.02(11)
O7A–Tb1–O6	148.25(10)	O11A–K1–O10	124.34(11)
O2B–Tb1–O6	74.92(9)	O3–K1–O6	60.83(8)
O1C–Tb1–O6	70.69(10)	O2B–K1–O6	62.39(8)
O3–Tb1–O6	71.98(9)	O4A–K1–O6	155.98(9)
O5–Tb1–O6	52.20(9)	O5A–K1–O6	138.71(8)
O11–Tb1–O6	125.72(10)	O11A–K1–O6	129.35(9)
O12–Tb1–O6	125.25(9)	O10–K1–O6	76.18(10)
O7A–Tb1–O4	68.97(10)	O3–K1–O9	120.17(14)
O2B–Tb1–O4	123.31(9)	O2B–K1–O9	136.94(13)
O1C–Tb1–O4	133.01(9)	O4A–K1–O9	91.67(13)
O3–Tb1–O4	50.30(9)	O5A–K1–O9	131.37(13)
O5–Tb1–O4	66.43(9)	O11A–K1–O9	65.30(13)
O11–Tb1–O4	74.82(9)	O10–K1–O9	72.62(14)
O12–Tb1–O4	132.12(9)	O6–K1–O9	82.74(13)
O6–Tb1–O4	102.58(9)		
Complex **3**[c]			
O3A–Tb1–O3	157.09(15)	O1A–Tb1–O1	71.23(14)
O3A–Tb1–O4B	103.27(11)	O3A–Tb1–O2	75.23(10)
O3–Tb1–O4B	83.95(11)	O3–Tb1–O2	127.58(10)
O3A–Tb1–O4C	83.95(11)	O4B–Tb1–O2	73.64(9)
O3–Tb1–O4C	103.27(11)	O4C–Tb1–O2	73.92(9)
O4B–Tb1–O4C	143.57(13)	O1A–Tb1–O2	143.50(9)
O3A–Tb1–O1A	84.49(13)	O1–Tb1–O2	130.46(11)
O3–Tb1–O1A	76.89(12)	O3A–Tb1–O2A	127.58(10)
O4B–Tb1–O1A	141.56(10)	O3–Tb1–O2A	75.23(10)
O4C–Tb1–O1A	74.03(9)	O4B–Tb1–O2A	73.92(9)
O3A–Tb1–O1	76.89(12)	O4C–Tb1–O2A	73.64(9)
O3–Tb1–O1	84.49(13)	O1A–Tb1–O2A	130.46(11)
O4B–Tb1–O1	74.03(9)	O1–Tb1–O2A	143.50(9)
O4C–Tb1–O1	141.56(10)	O2–Tb1–O2A	53.36(13)

[a] Symmetry transformations used to generate equivalent atoms: #1 $-x$, $y + 1/2$, $-z + 1$; #2 $-x$, $-y$, $-z + 1$; #3 $x - 1/2$, y, $-z + ½$; #4 $x - 1/2$, $-y + 1/2$, $-z + 1/2$; #5 $x + 1/2$, y, $-z + 1/2$; #6 x, $-y + 1/2$, z. [b] Symmetry transformations used to generate equivalent atoms: #1 $-x + 1/2$, $y - 1/2$, $-z + 3/2$; #2 x, $-y$, $z + 1/2$; #3 $-x + 1/2$, $y + 1/2$, $-z + 3/2$; #4 x, $-y$, $z - 1/2$. [c] Symmetry transformations used to generate equivalent atoms: #1 $-x + 1$, y, $-z + 3/2$; #2 x, $-y$, $z + ½$; #3 $-x + 1$, $-y$, $-z+1$.

analysis after filtering and washing with ethanol. Yield: 0.348 g (28%). IR (KBr): $\tilde{\nu}$ = 3403 (w), 3087 (w), 1690 (m), 1612 (s), 1531 (s), 1481 (m), 1453 (s), 1395 (s), 452 (w), 424 (w) cm^{-1}.

$[Tb(ina)_3(H_2O)_2]_n$ (3): A solution of $TbCl_3 \cdot 6H_2O$ (0.746 g, 2 mmol) in water (15 mL) was added dropwise to a solution of ina (0.7441 g, 6.05 mmol) dissolved in methanol (10 mL) and acetonitrile (10 mL) with stirring. The solution was continuously stirred for 30 min with a magnetic stirrer. The reaction mixture was neutralized to pH = 6.5 by using ethylenediamine. The solution was concentrated to 1/3 of its volume and cooled to afford a white precipitate. The reaction mixture was filtered, and the filtrate was left undisturbed to evaporate at room temperature over a period of 1 month to afford colourless stick crystals suitable for X-ray single crystal diffraction analysis after filtering and washing with methanol. Yield: 0.3375 g (33%). IR (KBr): $\tilde{\nu}$ = 3406 (m), 3052 (w), 1714 (s), 1614 (m), 1593 (m), 1548 (m), 1412 (vs1335 m), 1300 (s), 492 (m), 413 (w) cm^{-1}.

Crystal Data Collection and Refinement: Intensity data of complexes **1**, **2** and **3** were measured with a Rigaku-Raxis-IV X-ray diffractometer by using monochromated Mo-K_α (λ = 0.71073 Å) radiation at 293(2) K for complex **1**, 291(2) K for complex **2** and 291(2) K for complex **3**. Raw data were corrected and the structures were solved by using the SHELX-97 program. All non-hydrogen atoms were refined anisotropically by full-matrix least-squares methods. The full-matrix least-squares calculations on F^2 were applied on the final refinement. Details of the crystal structural determinations for complex **1**–**3** are summarized in Table 3 and their selected bond lengths and angles are listed in Tables 4 and 5.

CCDC-605585 (for **1**), -610138 (for **2**), and -633756 (for **3**) contain the supplementary crystallographic data for this paper. These data can be obtained free of charge from The Cambridge Crystallographic Data Centre via www.ccdc.cam.ac.uk/data_request/cif.

Supporting Information (see footnote on the first page of this article): TG–DTG curves of **1** and **3**.

Acknowledgments

We gratefully acknowledge financial support from the National Natural Science Foundation of China (20771094, 20671083) and the Science and Technology Key Task of Henan Province (0524270061).

[1] H. Abourahma, B. Moulton, V. Kravtsov, M. J. Zaworotko, *J. Am. Chem. Soc.* **2002**, *124*, 9990 –9991.
[2] M. Eddaoudi, J. Kim, N. Rosi, D. Vodak, J. Wachter, M. O'Keeffe, O. M. Yghi, *Science* **2002**, *295*, 469–472.
[3] H. Li, M. Eddaoudi, M. O'Keeffe, O. M. Yghi, *Nature* **1999**, *402*, 276–279.
[4] L. Xu, G. C. Guo, B. Liu, M. S. Wang, J. S. Huang, *Inorg. Chem. Commun.* **2004**, *7*, 1145–1149.
[5] a) S. A. Boume, J. J. Lu, A. Mondal, B. Moulton, M. J. Zaworotko, *Angew. Chem. Int. Ed.* **2001**, *40*, 2111–2113; b) D. T. Vodak, M. E. Braun, J. Kim, M. Edlaoudi, O. M. Yaghi, *Chem. Commun.* **2001**, 2534 –2535.
[6] a) S. Y. Yang, L. S. Long, R. B. Huang, L. S. Zheng, *Chem. Commun.* **2002**, 472–473; b) C. B. Ma, C. N. Chen, Q. T. Liu, D. Z. Liao, L. C. Li, L. C. Sun, *New J. Chem.* **2003**, *27*, 890–894.
[7] a) B. Moulton, H. Abourahma, M. W. Bradner, J. J. Lu, G. J. McManus, M. J. Zaworotko, *Chem. Commun.* **2003**, 1342–1343; b) Y. H. Wan, L. P. Zhang, L. P. Jin, S. Gao, S. Z. Lu, *Inorg. Chem.* **2003**, *42*, 4985–4994.
[8] a) L. Y. Zhang, G. F. Liu, S. L. Zheng, B. H. Ye, X. M. Zhang, X. M. Cheng, *Eur. J. Inorg. Chem.* **2003**, 2965–2971; b) N. J. Burke, A. D. Burrows, A. S. Donovan, R. W. Harrington, M. F. Mahon, C. F. Price, *Dalton Trans.* **2003**, 3840–3849.
[9] Y. L. Qu, Y. X. Ke, S. M. Lu, R. Fan, G. Q. Pan, J. M. Li, *J. Mol. Struct.* **2005**, *734*, 7–13.
[10] a) A. J. Blake, N. R. Champness, A. Khlobystov, W. S. Li, M. Schroder, A. Khlobystov, D. A. Lemenovskii, *Chem. Commun.* **1997**, 2027–2028; b) L. N. Zhu, L. Zhang, W. Z. Wang, D. Z. Liao, P. Cheng, Z. H. Jiang, S. P. Yan, *Inorg. Chem. Commun.* **2002**, *5*, 1017–1021.
[11] a) L. Pan, N. W. Zheng, Y. G. Wu, Y. G. Wu, S. Han, R. Y. Yang, X. Y. Huang, J. Li, *Inorg. Chem.* **2001**, *40*, 828–830; b) L. Pan, X. Y. Huang, J. Li, Y. G. Wu, N. W. Zheng, *Angew. Chem. Int. Ed.* **2000**, *39*, 527–530.
[12] a) X. Li, Z. Q. Bian, L. P. Jin, S. Z. Lu, S. H. Huang, *J. Mol. Struct.* **2000**, *522*, 117–123; b) M. C. Yin, C. C. Ai, L. J. Yuan, C. W. Wang, J. T. Sun, *J. Mol. Struct.* **2004**, *691*, 33–37.
[13] L. j. Yuan, M. C. Yin, E. T. Yuan, J. T. Sun, K. L. Zhang, *Inorg. Chim. Acta* **2004**, *357*, 89–94.
[14] S. C. J. Meskers, M. Ubbink, G. W. Canters, H. P. J. M. Dekkers, *J. Bio. Inorg. Chem.* **1998**, *3*, 463–469.
[15] S. Capecchi, O. Renauit, D. G. Moon, M. Halim, M. Etchells, P. J. Dobson, O. V. Salata, V. Christou, *Adv. Mater.* **2000**, *12*, 1591–1594.
[16] M. H. V. Werts, M. A. Duin, J. W. Hofstraat, J. W. Verhoeven, *Chem. Commun.* **1999**, 799–800.
[17] M. C. Yin, L. J. Yuan, C. C. Ai, C. W. Wang, E. T. Yuan, J. T. Sun, *Polyhedron* **2004**, *23*, 529–536.
[18] A. P. de Silva, H. Q. N. Gunaratne, T. Gunnlaugsson, A. J. M. Huxley, C. P. McCoy, J. T. Rademacher, T. E. Rice, *Chem. Rev.* **1997**, *97*, 1515–1566.
[19] C. Yang, X. M. Chen, W. H. Zhang, J. Chen, Y. S. Yang, M. L. Gong, *J. Chem. Soc., Dalton Trans.* **1996**, 1767–1768.
[20] J. C. G. Bünzli, F. Ihringer, *Inorg. Chim. Acta* **1996**, *246*, 195–205.
[21] J. B. Lamture, Z. H. Zhou, A. S. Kumar, T. G. Wensel, *Inorg. Chem.* **1995**, *34*, 864–869.
[22] S. Petoud, J. C. G. Buenzli, K. J. Schenk, C. Piguet, *Inorg. Chem.* **1997**, *36*, 1345–1353.
[23] A. de Bettencourt-Dias, *Inorg. Chem.* **2005**, *44*, 2734–2741.
[24] A. W. H. Lam, W. T. Wong, S. Gao, G. H. Wen, X. X. Zhang, *Eur. J. Inorg. Chem.* **2003**, 149–163.
[25] C. Seward, N. X. Hu, S. Wang, *J. Chem. Soc., Dalton Trans.* **2001**, 134–137.
[26] X. Li, X. Zheng, L. Jin, S. Lu, W. Qin, *J. Mol. Struct.* **2000**, *519*, 85–91.
[27] B. Barja, R. Baggio, M. T. Garland, P. F. Aramendia, O. Pena, M. Perec, *Inorg. Chim. Acta* **2003**, *346*, 187–196.
[28] Y. B. Wang, W. J. Zhuang, L. P. Jin, S. Z. Lu, *J. Mol. Struct.* **2004**, *705*, 21–27.
[29] Y. B. Wang, X. J. Zheng, W. J. Zhuang, L. P. Jin, *Eur. J. Inorg. Chem.* **2003**, 1355–1360.
[30] B. Zhao, X. Y. Chen, P. Cheng, D. Z. Liao, S. P. Yan, Z. H. Jiang, *J. Am. Chem. Soc.* **2004**, *126*, 15394–15395.
[31] Y. X. Zhou, X. Q. Shen, H. L. Liu, H. Y. Zhang, Q. A. Wu, Y. Zhu, H. W. Hou, *Synth. React. Inorg. Met.-Org. Chem.* **2006**, *36*, 563–568.
[32] a) B. Q. Ma, H. L. Sun, S. Gao, *Chem. Commun.* **2004**, 2220–2221; b) Y. C. Liao, Y. C. Jiang, S. L. Wang, *J. Am. Chem. Soc.* **2005**, *127*, 12794–12795; c) M. Yoshizawa, T. Kusukawa, M. Kawano, T. Ohhara, I. Tanaka, K. Kurihara, N. Niimura, M. Fujita, *J. Am. Chem. Soc.* **2005**, *127*, 2798–2799; d) P. S. Lakshminarayanan, E. Suresh, P. Ghosh, *Angew. Chem. Int. Ed.* **2006**, *45*, 3807–3811.
[33] X. Q. Shen, H. J. Zhong, H. Zheng, H. Y. Zhang, G. H. Zhao, Q. A. Wu, H. Y. Mao, E. B. Wang, Y. Zhu, *Polyhedron* **2004**, *23*, 1851–1857.
[34] T. Ozawa, *Bull. Chem. Soc. Jpn.* **1965**, *38*, 1881–1886.

[35] B. Barja, R. Baggio, M. T. Garland, P. F. Aramendia, O. Pena, M. Perec, *Inorg. Chim. Acta* **2003**, *346*, 187–196.
[36] K. B. Yatsimirskii, N. K. Davidenko, *Coord. Chem. Rev.* **1979**, *27*, 223–273.
[37] N. Arnaud, E. Vaquer, J. Georges, *Analyst* **1998**, *123*, 261–265.
[38] C. H. Huang, *Rare Earth Coordination Chemistry*, Science Press, Beijing, China, **1997**, p. 363 (in Chinese).
[39] L. Oyang, H. L. Sun, X. Y. Wang, J. R. Li, D. B. Nie, W. F. Fu, S. Gao, K. B. Yu, *J. Mol. Struct.* **2005**, *740*, 175–180.
[40] J. J. An, Z. C. Chen, *Translation of Handbook on the Synthesis of Inorganic Compounds*, Chemical Society of Japan, **1986**, vol. II, p. 261.

Received: April 28, 2008
Published Online: August 15, 2008

